THE JOURNAL OF PHYSICAL CHEMISTRY Letters

Letter

pubs.acs.org/JPCL

Structural Relaxation of Low-Density Amorphous Ice upon Thermal Annealing

Jacob J. Shephard,[†,‡] John S. O. Evans,[‡] and Christoph G. Salzmann*[,†]

[†]Department of Chemistry, University College London, 20 Gordon Street, London WC1H 0AJ, United Kingdom

[‡]Department of Chemistry, Durham University, South Road, Durham DH1 3LE, United Kingdom

ABSTRACT: Despite the importance of low-density amorphous ice (LDA) in critical cosmological processes and its prominence as one of the polyamorphs of water there is still an incomplete picture of the processes that take place upon thermal annealing. Using Raman and Fourier transform infrared (FT-IR) spectroscopy, we show that a gradual structural relaxation process takes place upon heating vapor-deposited LDA, also called amorphous solid water, and LDAs obtained from several different states of high-density amorphous ice. The relaxation leads to an increase in structural order on local and more extended length scales as the average O−O distance shortens and the O−O distance distribution narrows. The relaxation process is separate from crystallization, and it does not seem to reach completion before crystallization sets in. Our findings are difficult to reconcile with the postulated glass transition of LDA to the supercooled and highly viscous liquid *prior* to crystallization.

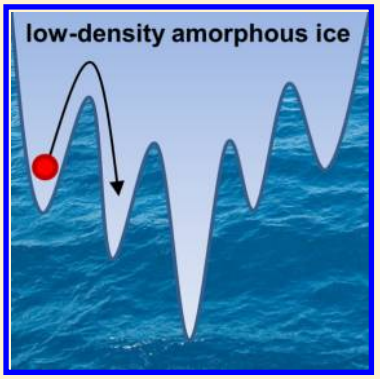

SECTION: Glasses, Colloids, Polymers, and Soft Matter

Low-density amorphous ice (LDA) is one of the polyamorphs of ice[1−3] and, as the most prevailing form of ice in the Universe, is involved in a wide range of cosmological processes.[4] LDA can be prepared by vapor deposition (amorphous solid water, ASW),[5−7] hyper-quenching of small water droplets (hyper-quenched glassy water, HGW),[8−10] or by decompression or heating of high-density amorphous ice (HDA).[1,2] It has been argued that LDA obtained from HDA is structurally different from ASW and HGW,[11−14] which were found to have similar structures.[11,15] While LDA from HDA has been considered to be fully relaxed at 120 K,[16] a range of structurally different LDAs have been observed immediately after the transformation from HDA.[17] Using neutron diffraction with isotopic substitution, it has been shown that LDA from HDA, ASW, and HGW have identical structures.[18] Later, however, two states of LDA, LDA-I and LDA-II, with subtle structural differences were identified.[19] LDA-I is obtained by ambient-pressure heating of uHDA, the unannealed state of HDA made via pressure-induced amorphization of ice I at 77 K.[1,20] The preparation of LDA-II involves converting uHDA to very high-density amorphous ice (vHDA) in a first step by heating at pressures greater than 0.8 GPa[21,22] and isothermal decompression at 140 K, which proceeds via the expanded high-density amorphous ice (eHDA) state.[20,23] The same LDA-II state can be obtained by heating eHDA at ambient pressure.[24]

On the basis of a reversible heat-capacity increase, it has been postulated that the glass transition of LDA to the supercooled liquid takes place *prior* to crystallization at 136 K upon heating at 30 K min^{-1} and at 124 K at 0.17 K min^{-1}.[15,25−27] Several studies have been presented in support of this scenario.[24,28−32] However, it has also been argued that the true glass transition of water should be at considerably higher temperatures.[33−35] To complicate matters further, there are also studies pointing toward a more 'crystal-like' nature of LDA.[13,36−42] In summary, there is currently no generally accepted view of the structural nature of LDA and of the processes that occur upon heating. In particular, questions related to if, how, and why the properties of LDA depend on the way in which it is prepared need to be answered.

Here we use Raman and Fourier transform infrared (FT-IR) spectroscopy to search for structural relaxation processes upon heating as-made ASW and LDAs obtained from uHDA, eHDA and vHDA. The results for these four kinds of LDA are compared, and we discuss whether our findings can be reconciled with the postulated glass transition *prior* to crystallization.[15,25]

The Raman spectrum of as-made ASW in the region of the ν(OH) stretching modes is shown as spectrum (1) in Figure 1a. In order to investigate the effects of thermal annealing on the structure of ASW Raman spectra were recorded at 80 K after samples were heated to successively higher temperatures. This temperature profile enabled the irreversible spectral changes, which take place during the annealing steps, to be separated from the spectral effects of thermal expansion.

Annealing processes are clearly evident in these spectra as a peak shift of the most intense feature from 3116 cm^{-1} for as-made ASW to 3098 cm^{-1} after annealing at 145 K (cf. Figure 2a). Upon annealing at 155 K, the sample crystallized and the Raman spectrum of ice I was obtained.[43] In addition to these

Received: September 17, 2013
Accepted: October 14, 2013
Published: October 14, 2013

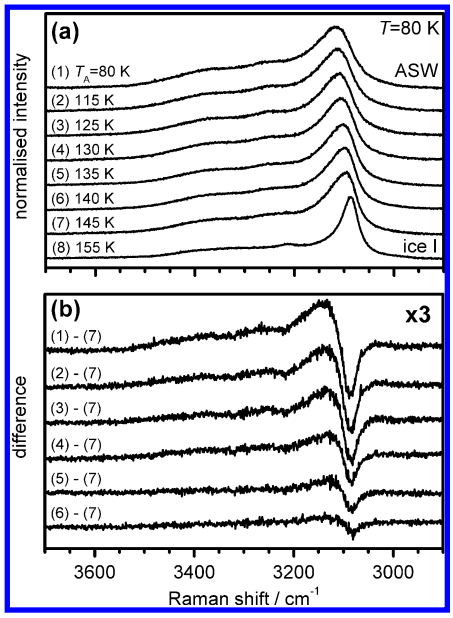

Figure 1. (a) Raman spectra of the coupled ν(OH) region of annealed ASW normalized to the maximum intensity of the most intense feature. (b) Differences between spectra 1−6 and spectrum 7 in panel (a).

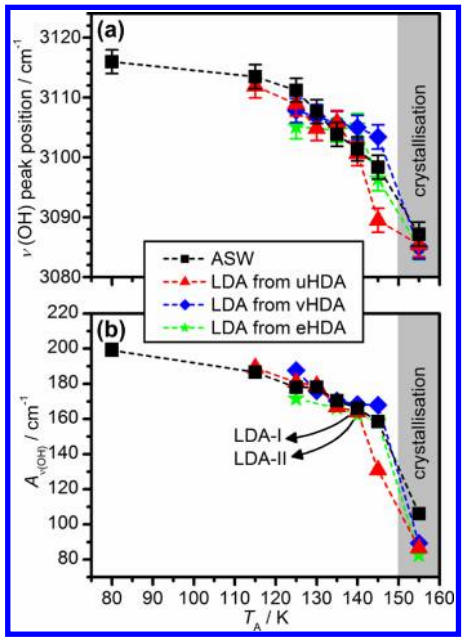

Figure 2. ν(O−H) peak positions (a) and integrated ν(O−H) peak areas (b) of various LDA samples as a function of the annealing temperature. The size of the symbols in (b) reflects the margins of error.

peak shifts, changes in shape of the spectral features were observed upon annealing, which are shown more clearly in the difference spectra of Figure 1b. The changes can be summarized as a sharpening of the main feature, which is more pronounced on the high-frequency side, and a decrease in the relative intensities of the shoulders at ∼3265 and ∼3380 cm^{-1}.

In a next step, the peak areas of the entire ν(OH) feature, $A_{\nu(OH)}$, were determined. This quantity captures the sharpening of the main feature as well as the relative intensity decreases of the shoulders, and is therefore highly sensitive toward the structural changes upon annealing. Figure 2b shows a plot of $A_{\nu(OH)}$ as a function of the annealing temperature. It can be seen that the annealing leads to gradual spectroscopic changes which increase in magnitude toward higher annealing temperatures.

The stretching modes in ice are strongly affected by intermolecular coupling processes.[43] In general, the most intense feature in the ν(OH) region of the Raman spectrum of crystalline and amorphous ice is assigned to the intermolecularly coupled symmetric stretching of all water molecules vibrating in phase.[43,44] Much of our understanding of the Raman spectroscopic properties of ice has come from analyzing the Raman spectrum of the high-symmetry ice VIII, which is the only known case where mixing of the symmetric and antisymmetric stretching modes of neighboring water molecules is not permitted due to their different symmetry species.[43−45] For the lower-symmetry ice XV,[46] all Raman-active modes have A_{1g} character, which allows mixing of symmetric and antisymmetric stretching modes.[44] In analogy to this, amorphous ice, displaying no long-range order or symmetry, is also expected to permit mixing of symmetric and antisymmetric stretching of neighboring water molecules. The high-frequency shoulders of the ν(OH) band are therefore thought to originate from such mixed and coupled stretching modes. Additional contributions from Fermi resonances or coupling with bending or phonon modes may also be important.[47−49]

Due to the coupled nature of the ν(OH) modes, changes in this spectral region reflect structural changes of the hydrogen-bonded network on a length scale longer than the local first-neighbor environment. Whalley has stated that at least 25 molecules take part in the coupled symmetric ν(OH) stretching of ice *Ih*.[43] For liquid water, the coupling of the stretching modes is thought to extend over 10 or more molecules,[50] and it can be assumed that the situation is similar for amorphous ice.

Thus, the sharpening of the symmetric ν(OH) stretching mode upon annealing implies that as-made ASW is structurally less ordered, over length scales comparable to the coupling, than the states immediately *prior* to crystallization (i.e., the molecules are in structurally more diverse environments in the as-made ASW).

The coupling of the stretching modes in H_2O ice can be 'switched off' by introducing deuterium as an isotopic impurity. Due to the substantial frequency mismatch between O−H and O−D oscillators, and the low concentrations of the O−D oscillators, decoupled μ(O−D) modes can be observed.[51] To obtain high signal-to-noise (S/N) ratio spectra of the μ(O−D), we have recorded FT-IR spectra of 91.0 mol % H_2O + 9.0 mol % HDO ASW films (cf. Figure 3a). The spectroscopic selection rules of the μ(O−D) modes are the same for IR and Raman, and it has been shown that the spectroscopic information obtained from IR or Raman is identical.[51]

Due to the localized nature of the decoupled μ(O−D) modes, spectral changes reflect structural changes in the first-neighbor environment (i.e., changes in local O−O distances and O−O−O angles). A decrease in peak position and sharpening of the μ(O−D) peak is observed upon annealing ASW as shown in Figure 3b. The feature in the spectrum recorded after annealing at 140 K is comprised of two components due to ASW and some additional ice I. Peak-fitting with two pseudo-Voigt functions revealed that the trend of decreasing peak positions and half-widths continues to this

dx.doi.org/10.1021/jz4020103 | J. Phys. Chem. Lett. 2013, 4, 3672−3676

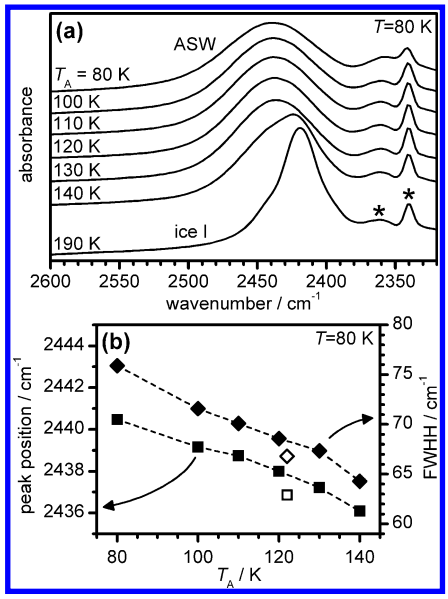

Figure 3. (a) FT-IR spectra of the decoupled μ(OD) region of annealed ASW (91.0 mol % H_2O + 9.0 mol % HDO). Asterisks indicate peaks associated with gaseous CO_2 in the spectrometer housing. (b) Peak positions and full-widths-at-half-heights of the ASW spectra in (a), obtained by peak-fitting with pseudo-Voigt functions. The data indicated by the open symbols were obtained after annealing at 122 K for 2 h in a separate experiment.

annealing temperature. Annealing at 150 K finally leads to a completely crystallized sample.

Several correlations between the μ(O−D) frequency and the hydrogen-bonded O−O distance have been reported (reviewed in ref 52). Using the correlation from ref 11 the peak positions in Figure 3b would correspond to a reduction in average O−O distance from 2.783 Å, for as-made ASW, to 2.779 Å after annealing at 130 K. Furthermore, the decrease in half-width of the μ(O−D) peak implies that the O−O distance distribution narrows upon annealing.

It is interesting to note that the changes in the μ(O−D) peak position are an almost linear function of the annealing temperature, whereas the changes in ν(OH) were found to 'drop off' as the annealing temperature was increased (cf. Figure 2). This could be interpreted as arising from the different length scales probed in the two measurements, due to the (de)coupling of vibrational modes (i.e., substantial increases in local order may be required for the more extended length scale to be affected significantly). X-ray diffraction data of ASW annealed at 115 K has shown a sharpening of the first strong diffraction peak compared to the as-made sample.[15] We assume that this is caused by the same structural relaxation process identified here.

It has previously been shown that as-made ASW is a highly microporous material and that significant sintering and loss of porosity occurs upon annealing.[15,53] It seems unlikely that sintering processes, which manifest on very long length scales, could cause the spectroscopic changes observed here. However, to exclude this possibility we have also studied the effects of thermal annealing on LDA obtained from various kinds of HDA. Sintering processes can be excluded for these samples.

In order to transform uHDA, vHDA, and eHDA to LDA the samples were heated while continuously recording spectra in the ν(OH) region to observe the transition. The transition temperatures to LDA were found at ∼110 K (uHDA), ∼118 K (vHDA), and ∼122 K (eHDA).[54,55] The obtained LDA samples were then subjected to the same thermal cycling as the ASW samples. As before, the spectra of the annealed LDAs were analyzed with respect to the ν(OH) peak positions and the $A_{\nu(OH)}$ (cf. Figure 2).

The peak positions and the $A_{\nu(OH)}$ values of the LDAs from the various HDAs follow a similar trend to ASW. We note that Suzuki et al. have reported a similar trend for the ν(OH) peak position of LDA from uHDA.[56] Also, the changes in the shape of the ν(OH) feature with increasing annealing temperature were found to be very similar for the LDAs from the HDAs compared to ASW. The deviations in $A_{\nu(OH)}$ at 125 K for LDA from eHDA and vHDA may be significant, indicating that the state of relaxation of these LDAs may be different from each other immediately after the transitions from the HDAs. However, after annealing at 130, 135, and 140 K the values of $A_{\nu(OH)}$ for all of the LDAs studied here were identical within experimental error. This shows that very similar gradual structural relaxation processes take place in the LDAs from the HDAs and in ASW. All four amorphous samples can therefore be considered to be structurally very similar for a given annealing temperature and time, at least after annealing above 130 K. Differences after annealing at 145 K are associated with partial crystallization of the less thermally stable LDAs.

Based on the data shown in Figure 2, it is not possible to differentiate between the LDA-I and LDA-II states, which were found to have different structures using neutron diffraction.[19] One explanation for the discrepancy could be that neutron diffraction is more sensitive at detecting subtle structural differences than vibrational spectroscopy. Alternatively, we suggest that the LDA-II sample in ref 19 may have been more relaxed, as it spent more time at 140 K during decompression than the LDA-I sample, which was heated to 140 K and immediately cooled back to 80 K. The time dependence of the relaxation process is demonstrated by the changes in peak position and half-width after annealing for 2 h at 122 K (cf. Figure 3b).

In summary, we have shown that ASW as well as LDA from uHDA, eHDA, and vHDA undergo gradual structural relaxation processes upon thermal annealing. The annealing leads to very similar increases in structural order of the hydrogen-bonded networks. Since LDA and ice I were found to coexist during crystallization, it seems as if the structural relaxation and crystallization are different processes. The relaxation process does not seem to have come to completion before crystallization sets in, indicating that the bottom of the LDA mega-basin may be hard to reach.

It is difficult to reconcile our findings with the postulated glass transition of LDA to the supercooled liquid before the onset of crystallization.[15,25] By definition, after heating above a glass transition temperature a sample is in (metastable) equilibrium on the experimental time scale. This should bring the structural relaxation process to completion which would manifest in leveling off of the spectroscopic quantities shown in Figures 2 and 3b.

Comparisons of the calorimetric data of LDA with those of some of the crystalline phases of ice[57−59] have recently led to the proposition that the calorimetric feature of LDA *prior* to crystallization may be connected to kinetic unfreezing of defect-migration mediated reorientation dynamics.[60] As changes in reorientation dynamics do not require reconstructions of the oxygen network, the relaxation process observed here could take place independently of reorientation processes. It seems

dx.doi.org/10.1021/jz4020103 | J. Phys. Chem. Lett. 2013, 4, 3672−3676

possible that LDA may in fact have two "glass transitions": one corresponding to the unfreezing of reorientation dynamics *prior* to crystallization, and another one at higher temperatures due to the transition to the supercooled and highly viscous liquid.

EXPERIMENTAL METHODS

ASW was prepared in a purpose-built vacuum chamber by depositing water vapor onto substrates maintained at 80 K using a leak rate of 0.4 g h^{-1}. Compression of ice I*h* at 77 K to 1.7 GPa in a pressure die produced uHDA.[1] The conversion of uHDA to either eHDA or vHDA was achieved by heating from 77 to 130 or 155 K at 0.3 or 1.4 GPa, respectively. Once the target temperatures had been reached the samples were quenched and recovered at ambient pressure under liquid nitrogen.

Raman spectra of the samples were recorded using an Oxford Microstat^{N} cryostat and a Renishaw Ramascope spectrometer (632.8 nm). For annealing, the cryostat was heated at ∼5 K min^{-1} from 80 K to a given annealing temperature followed by immediate cooling back to 80 K. FT-IR spectra were recorded from ASW films deposited onto MgF_2 discs using the same cryostat and an ATI Mattson Research Series 1 spectrometer (4 cm^{-1} spectral resolution). For annealing, the cryostat was heated to a given annealing temperature, kept at this temperature for 4 min, and cooled back to 80 K. A background spectrum was obtained after evaporating the ice at 260 K.

AUTHOR INFORMATION

Corresponding Author

*E-mail: c.salzmann@ucl.ac.uk.

Notes

The authors declare no competing financial interest.

ACKNOWLEDGMENTS

We thank the Royal Society for a University Research Fellowship (C.G.S.) and the EPSRC for a studentship (J.J.S.).

REFERENCES

(1) Mishima, O.; Calvert, L. D.; Whalley, E. 'Melting Ice' I at 77 K and 10 kbar: A New Method of Making Amorphous Solids. *Nature* **1984**, *310*, 393−395.

(2) Mishima, O.; Calvert, L. D.; Whalley, E. An Apparently First-Order Transition Between Two Amorphous Phases of Ice Induced by Pressure. *Nature* **1985**, *314*, 76−78.

(3) Loerting, T.; Winkel, K.; Seidl, M.; Bauer, M.; Mitterdorfer, C.; Handle, P. H.; Salzmann, C. G.; Mayer, E.; Finney, J. L.; Bowron, D. T. How Many Amorphous Ices Are There? *Phys. Chem. Chem. Phys.* **2011**, *13*, 8783−8794.

(4) Kwok, S. *Physics and Chemistry of the Interstellar Medium*; University Science Books: Sausalito, CA; 2007.

(5) Burton, E. F.; Oliver, W. F. The Crystal Structure of Ice at Low Temperatures. *Proc. R. Soc. London, Ser. A* **1935**, *153*, 166−172.

(6) Burton, E. F.; Oliver, W. F. X-ray Diffraction Patterns of Ice. *Nature* **1935**, *135*, 505−506.

(7) Jenniskens, P.; Blake, D. F. Structural Transitions in Amorphous Water Ice and Astrophysical Implications. *Science* **1994**, *265*, 753−756.

(8) Brüggeller, P.; Mayer, E. Complete Vitrification in Pure Liquid Water and Dilute Aqueous Solutions. *Nature* **1980**, *288*, 569−571.

(9) Mayer, E.; Brüggeller, P. Vitrification of Pure Liquid Water by High-Pressure Jet-Freezing. *Nature* **1982**, *298*, 715−718.

(10) Mayer, E. New Method for Vitrifying Water and Other Liquids by Rapid Cooling of Their Aerosols. *J. Appl. Phys.* **1985**, *58*, 663−667.

(11) Tulk, C. A.; Klug, D. D.; Branderhorst, R.; Sharpe, P.; Ripmeester, J. A. Hydrogen Bonding in Glassy Liquid Water from Raman Spectroscopic Studies. *J. Chem. Phys.* **1998**, *109*, 8478−8484.

(12) Klug, D. D.; Tulk, C. A.; Svensson, E. C.; Loong, C. K. Dynamics and Structural Details of Amorphous Phases of Ice Determined by Incoherent Inelastic Neutron-Scattering. *Phys. Rev. Lett.* **1999**, *83*, 2584−2587.

(13) Andersson, O.; Inaba, A. Thermal Conductivity of Cystalline and Amorphous Ices and Its Implications on Amorphization and Glassy Water. *Phys. Chem. Chem. Phys.* **2005**, *7*, 1441−1449.

(14) Johari, G. P. An Estimate for the Gibbs Energy of Amorphous Solid Waters and Differences between the Low-Density Amorph and Glassy Water. *J. Chem. Phys.* **2000**, *112*, 8573−8580.

(15) Hallbrucker, A.; Mayer, E.; Johari, G. P. Glass-Liquid Transition and the Enthalpy of Devitrification of Annealed Vapor-Deposited Amorphous Solid Water: A Comparison with Hyperquenched Glassy Water. *J. Phys. Chem.* **1989**, *93*, 4986−4990.

(16) Urquidi, J.; Benmore, C. J.; Neuefeind, J.; Tomberli, B.; Tulk, C. A.; Guthrie, M.; Egelstaff, P. A.; Klug, D. D. Isotopic Quantum Effects on the Structure of Low Density Amorphous Ice. *J. Phys.: Condens. Matter* **2003**, *15*, 3657−3664.

(17) Koza, M. M.; Schober, H.; Fischer, H. E.; Hansen, T.; Fujara, F. Kinetics of the High- to Low-density Amorphous Water Transition. *J. Phys.: Condens. Matter* **2003**, *15*, 321−332.

(18) Bowron, D. T.; Finney, J. L.; Hallbrucker, A.; Kohl, I.; Loerting, T.; Soper, A. K. The Local and Intermediate Range Structures of the Five Amorphous Ices at 80 K and Ambient Pressure: A Faber−Ziman and Bhatia−Thornton analysis. *J. Chem. Phys.* **2006**, *125*, 194502.

(19) Winkel, K.; Bowron, D. T.; Loerting, T.; Mayer, E.; Finney, J. L. Relaxation Effects in Low Density Amorphous Ice: Two Distinct Structural States Observed by Neutron Diffraction. *J. Chem. Phys.* **2009**, *130*, 204502.

(20) Nelmes, R. J.; Loveday, J. S.; Strässle, T.; Bull, C. L.; Guthrie, M.; Hamel, G.; Klotz, S. Annealed High-Density Amorphous Ice under Pressure. *Nat. Phys.* **2006**, *2*, 414−418.

(21) Loerting, T.; Salzmann, C.; Kohl, I.; Mayer, E.; Hallbrucker, A. A Second Distinct Structural "State" of High-density Amorphous Ice at 77 K and 1 bar. *Phys. Chem. Chem. Phys.* **2001**, *3*, 5355−5357.

(22) Salzmann, C. G.; Loerting, T.; Klotz, S.; Mirwald, P. W.; Hallbrucker, A.; Mayer, E. Isobaric Annealing of High-Density Amorphous Ice between 0.3 and 1.9 GPa: In Situ Density Values and Structural Changes. *Phys. Chem. Chem. Phys.* **2006**, *8*, 386−397.

(23) Winkel, K.; Elsaesser, M. S.; E., M.; T., L. Water Polyamorphism: Reversibility and (Dis)continuity. *J. Chem. Phys.* **2008**, *128*, 044510.

(24) Amann-Winkel, K.; Löw, F.; Handle, P. H.; Knoll, W.; Peters, J.; Geil, B.; Fujara, F.; T., L. Limits of Metastability in Amorphous Ices: The Neutron Scattering Debye−Waller Factor. *Phys. Chem. Chem. Phys.* **2013**, *14*, 16386−16391.

(25) Johari, G. P.; Hallbrucker, A.; Mayer, E. The Glass−Liquid Transition of Hyperquenched Water. *Nature* **1987**, *330*, 552−553.

(26) Hallbrucker, A.; Mayer, E.; Johari, G. P. The Heat Capacity and Glass Transition of Hyperquenched Glassy Water. *Philos. Mag. B* **1989**, *60*, 179−187.

(27) Handa, Y. P.; Klug, D. D. Heat Capacity and Glass Transition Behavior of Amorphous Ice. *J. Phys. Chem.* **1988**, *92*, 3323−3325.

(28) Johari, G. P. Liquid State of Low-Density Pressure-Amorphized Ice above Its T_g. *J. Phys. Chem. B* **1998**, *102*, 4711−4714.

(29) Smith, R. S.; Kay, B. D. The Existence of Supercooled Liquid Water at 150 K. *Nature* **1999**, *398*, 788−791.

(30) Seidl, M.; Elsaesser, M. S.; Winkel, K.; Zifferer, G.; Mayer, E.; Loerting, T. Volumetric Study Consistent with a Glass-to-Liquid Transition in Amorphous Ices under Pressure. *Phys. Rev. B* **2011**, *83*, 100201.

(31) Löw, F.; Amann-Winkel, K.; Loerting, T.; Fujara, F.; Geil, B. Ultra-slow Dynamics in Low Density Amorphous Ice Revealed by Deuteron NMR: Indication of a Glass Transition. *Phys. Chem. Chem. Phys.* **2013**, *15*, 9308−9314.

(32) Capaccioli, S.; Ngai, K. L. Resolving the Controversy on the Glass Transition Temperature of Water? *J. Chem. Phys.* **2011**, *135*, 104504.

(33) Velikov, V.; Borick, S.; Angell, C. A. The Glass Transition of Water, Based on Hyperquenching Experiments. *Science* **2001**, *294*, 2335−2338.
(34) Yue, Y.; Angell, C. A. Clarifying The Glass-Transition Behaviour of Water by Comparison with Hyperquenched Inorganic Glasses. *Nature* **2004**, *427*, 717−720.
(35) Angell, C. A. Insights into Phases of Liquid Water from Study of Its Unusual Glass-Forming Properties. *Science* **2008**, *319*, 582−587.
(36) Li, J.-C.; Jenniskens, P. Inelastic Neutron Scattering Study of High Density Amorphous Water Ice. *Planet. Space Sci.* **1997**, *45*, 469−473.
(37) Tse, J. S.; Klug, D. D.; Tulk, C. A.; Swainson, I.; Svensson, E. C.; Loong, C.-K.; Shpakov, V.; Belosludov, V. R.; Belosludov, R. V.; Kawazoe, Y. The Mechanisms for Pressure-Induced Amorphization of Ice Ih. *Nature* **1999**, *400*, 647−649.
(38) Schober, H.; Koza, M. M.; Tölle, A.; Masciovecchio, C.; Sette, F.; Fujara, F. Crystal-like High Frequency Phonons in the Amorphous Phases of Solid Water. *Phys. Rev. Lett.* **2000**, *85*, 4100−4103.
(39) Andersson, O.; Suga, H. Thermal Conductivity of Amorphous Ices. *Phys. Rev. B* **2002**, *65*, 140201.
(40) Geil, B.; Koza, M. M.; Fujara, F.; Schober, H.; Natali, F. Absence of Fast Precursor Dynamics of Low-Density Amorphous Ice around Its Hypothetical Glass Transition Temperature. *Phys. Chem. Chem. Phys.* **2004**, *6*, 677−679.
(41) Andersson, O. Dielectric Relaxation of Low-Density Amorphous Ice under Pressure. *Phys. Rev. Lett.* **2007**, *98*, 057602.
(42) Tse, J. S.; Shaw, D. M.; Klug, D. D.; Patchkovskii, S.; Vanko, G.; Monaco, G.; Krisch, M. X-ray Raman Spectroscopic Study of Water in the Condensed Phases. *Phys. Rev. Lett.* **2008**, *100*, 095502.
(43) Whalley, E. A Detailed Assignment of the O−H Stretching Bands of Ice I. *Can. J. Chem.* **1977**, *55*, 3429−3441.
(44) Whale, T. F.; Clark, S. J.; Finney, J. L.; Salzmann, C. G. DFT-Assisted Interpretation of the Raman Spectra of Hydrogen-Ordered Ice XV. *J. Raman Spectrosc.* **2013**, *44*, 290−298.
(45) Wong, P. T. T.; Whalley, E. Raman Spectrum of Ice VIII. *J. Chem. Phys.* **1976**, *64*, 2359−2366.
(46) Salzmann, C. G.; Radaelli, P. G.; Mayer, E.; Finney, J. L. Ice XV: A New Thermodynamically Stable Phase of Ice. *Phys. Rev. Lett.* **2009**, *103*, 105701.
(47) Perakis, F.; Hamm, P. Two-Dimensional Infrared Spectroscopy of Neat Ice Ih. *Phys. Chem. Chem. Phys.* **2012**, *14*, 6250−6256.
(48) Shi, L.; Gruenbaum, S. M.; Skinner, J. L. Interpretation of IR and Raman Line Shapes for H_2O and D_2O Ice Ih. *J. Phys. Chem. B* **2012**, *116*, 13821−13830.
(49) Shalit, A.; Perakis, F.; Hamm, P. Two-Dimensional Infrared Spectroscopy of Isotope-Diluted Low Density Amorphous Ice. *J. Phys. Chem. B* **2013**, DOI: 10.1021/jp4053743.
(50) Bakker, H. J.; Skinner, J. L. Vibrational Spectroscopy as a Probe of Structure and Dynamics in Liquid Water. *Chem. Rev.* **2010**, *110*, 1498−1517.
(51) Minceva-Sukarova, B.; Sherman, W. F.; Wilkinson, G. R. Isolated O−D Stretching Frequencies in Ice II. *Spectrochim. Acta* **1985**, *41A*, 315−318.
(52) Kuhs, W. F.; Lehmann, M. S. The Structure of Ice-Ih. In *Science Reviews 2*; Franks, F., Ed.; Cambridge University Press: Cambridge, U.K.; 1986, Vol. 2, pp 1−65.
(53) Mayer, E.; Pletzer, R. Astrophysical Implications of Amorphous Ice - A Microporous Solid. *Nature* **1986**, *319*, 298−301.
(54) Handa, Y. P.; Mishima, O.; Whalley, E. High-Density Amorphous Ice. III. Thermal Properties. *J. Chem. Phys.* **1986**, *84*, 2766−2770.
(55) Winkel, K.; Mayer, E.; Loerting, T. Equilibrated High-Density Amorphous Ice and Its First-Order Transition to the Low-Density Form. *J. Chem. Phys. B* **2011**, *115*, 14141−14148.
(56) Suzuki, Y.; Mishima, O. Raman Study of the Annealing Effect of Low-Density Glassy Waters. *J. Phys. Soc. Jpn.* **2003**, *72*, 3128−3131.
(57) Salzmann, C. G.; Kohl, I.; Loerting, T.; Mayer, E.; Hallbrucker, A. The Low-Temperature Dynamics of Recovered Ice XII As Studied by Differential Scanning Calorimetry: A Comparision with Ice V. *Phys. Chem. Chem. Phys.* **2003**, *5*, 3507−3517.
(58) Salzmann, C. G.; Mayer, E.; Hallbrucker, A. Thermal Properties of Metastable Ices IV and XII: Comparison, Isotope Effects and Relative Stabilities. *Phys. Chem. Chem. Phys.* **2004**, *6*, 1269−1276.
(59) Salzmann, C. G.; Radaelli, P. G.; Finney, J. L.; Mayer, E. A Calorimetric Study on the Low Temperature Dynamics of Doped Ice V and Its Reversible Phase Transition to Hydrogen Ordered Ice XIII. *Phys. Chem. Chem. Phys.* **2008**, *10*, 6313−6324.
(60) Salzmann, C. G.; Radaelli, P. G.; Slater, B.; Finney, J. L. The Polymorphism of Ice: Five Unresolved Questions. *Phys. Chem. Chem. Phys.* **2011**, *13*, 18468−18480.